Impact Analysis of FCS-MPC on Power Losses of IPMSM Drive fed by Cascaded H-Bridge Multilevel Inverter

Claudio Nevoloso
Department of Engineering
University of Palermo
Palermo, Italy
claudio.nevoloso@unipa.it

Gioacchino Scaglione
Department of Engineering
University of Palermo
Palermo, Italy
gioacchino.scaglione@unipa.it

Giuseppe Schettino
Department of Engineering
University of Palermo
Palermo, Italy
giuseppe.schettino@unipa.it

Antonino Oscar Di Tommaso
Department of Engineering
University of Palermo
Palermo, Italy
antoninooscar.ditommaso@unipa.it

Rosario Miceli
Department of Engineering
University of Palermo
Palermo, Italy
rosario.miceli@unipa.it

***Abstract*—This work aims to investigate the finite-control-set model predictive control impact on power losses and efficiency of an interior permanent magnet synchronous motor fed by a cascaded H-bridge multilevel inverter. This analysis is carried out by adopting the discrete Fourier transform approach, allowing motor power losses segregation into fundamental and harmonic power losses. To quantify finite-control-set model predictive control benefits, the standard field-oriented control strategy is adopted as a comparison target, and an experimental comparative analysis between such strategies is carried out on an interior permanent magnet synchronous motor drive fed by a cascaded H-bridge multilevel inverter. Comparison is carried out over 20 working points defined in the speed-torque plane at a fixed apparent switching frequency of 1.4 kHz. Experimental results prove that the model predictive control increases the motor efficiency in almost every working point, and most of the motor power losses are generated by fundamental quantities, implying additional margins for an overall efficiency improvement due to their controllability.**

Keywords— Model Predictive Control, Harmonic Power Losses, PMSM Drives, Cascaded H-Bridge Multilevel Inverters

I. INTRODUCTION

Electric drives represent one of the largest end-consumers of electricity, accounting for nearly 50% of all global electricity consumption [1]. The motor power losses represent the vast majority (more than 70%) of the total power losses in an electric drive [2]. Therefore, both scientific and industrial efforts focus on reducing motor power losses by employing new control algorithms and hardware solutions [3]-[6]. On the hardware side, Multilevel Inverters (MIs) are the main candidates in many medium-high-power applications and emerge as the primary candidates for reducing voltage and current harmonic distortion and motor power losses [7]-[9]. On the control side, Finite-Control-Set Model Predictive Control (FCS-MPC) is gaining considerable attention in the electric drives field due to its model-based multi-variable control approach that allows for accounting for the converter non-linearities and fulfilling several conflicting control goals [10]-[11]. According to [12]-[13], typical electric drive performance metrics are the current Total Demand Distortion (TDD) and the converter switching frequency. They are currently adopted to quantify the benefits of FCS-MPC over standard control strategies. However, such performance metrics do not accurately describe the interior permanent magnet synchronous motor (IPMSM) behaviour in terms of power losses or efficiency. In this context, the overwhelming majority of works in the scientific literature address the power losses analysis for variable-speed drives fed by conventional Two-Level Voltage Source Inverters (2L-VSIs) controlled with standard Field-Oriented Control (FOC) strategies [14]-[16], since it is the most widespread commercial technology. Since FCS-MPC is an emerging control strategy, power losses analysis is poorly investigated in the scientific literature, especially when MIs are adopted [17]-[20]. Moreover, it is necessary to take into account the medium voltage drives issue related to balancing the trade-off between electric drive efficiency and system performance when a low switching frequency is imposed to reduce switching losses and device stress. In detail, conventional MultiCarrier-PWM (MC-PWM) based FOC struggles to balance the described trade-off, but FCS-MPC allows for overcoming standard control limitations due to its multivariable control capability [21]. Thus, accurate performance analysis of FCS-MPC on MI-PMSM drives is a relevant topic due to FCS-MPC is an emerging and valid control candidate for industry applications with significant growth in its use in the coming years.

Given the above, this paper proposes an experimental analysis on a Three-Phase Five-Level Cascaded H-Bridge Multilevel Inverter (3P-5L-CHMI)-fed IPMSM drive controlled with FCS-MPC devoted to investigating the control impact on the IPMSM efficiency and power losses. Such an analysis is carried out by adopting the Discrete Fourier Transform (DFT) approach [22] that allows for segregating fundamental and harmonic power losses from measured total power losses. To accurately identify IPMSM loss maps, 20 IPMSM Working Points(WPs) are defined in the speed-torque plane. Furthermore, to quantify the IPMSM efficiency improvement derived from the use of FCS-MPC, a comparison with a conventional Phase Shifted Pulse Width Modulation (PS-PWM)-based FOC is accomplished under identical operating conditions at a fixed apparent switching frequency of 1.4 kHz. In this study, a novel FCS-MPC strategy for 3P-5L-CHBMI-fed IPMSM drive, proposed by the authors in [23], namely Voltage Vector-based (V^2B) FCS-MPC, is employed for the mentioned performance comparison analysis.

The paper is structured as follows: Section II describes the main features of control strategies considered for comparative analysis; Section III presents the harmonic power analysis approach used for IPMSM power losses segregation; Section IV describes the test bench and the CHBMI-fed IPMSM drive under test; Section V presents the experimental investigations and discusses the related results. Finally, section VI summarizes the analysis and conclusions of this work.

II. FCS-MPC AND FOC STRATEGIES

This section summarizes the main features of the V^2B FCS-MPC strategy [23] and the standard FOC strategy adopted for comparative analysis purposes.

A. Voltage Vector-Based Model Predictive Control

The V^2B-MPC is a multiobjective control strategy that allows for fulfilling the following goals: computational burden minimization; Commode Mode Voltages (CMVs) minimization; Gate Control Signals (GCS) transitions minimization; phase voltages *dv/dt* minimization. The control strategy is formulated based on the IPMSM continuous-time state-space model in the *d-q* reference frame reported below:

$$\frac{d}{dt}\boldsymbol{i}_{dq}(t) = \boldsymbol{F}\boldsymbol{i}_{dq}(t) + \boldsymbol{G}\boldsymbol{v}_{dq}(t) + \boldsymbol{H} \tag{1}$$

with:

$$\boldsymbol{F} = \begin{bmatrix} -\frac{R}{L_d} & \frac{p\omega_m L_q}{L_d} \\ -\frac{p\omega_m L_d}{L_q} & -\frac{R}{L_q} \end{bmatrix}; \boldsymbol{G} = \begin{bmatrix} \frac{1}{L_d} & 0 \\ 0 & \frac{1}{L_q} \end{bmatrix}; \boldsymbol{H} = \begin{bmatrix} 0 \\ -\frac{p\omega_m \lambda_{PM}}{L_q} \end{bmatrix} \tag{2}$$

where $v_{dq}=[v_d\ v_q]^T$ is the stator voltage vector and $i_{dq}=[i_d\ i_q]^T$ is the stator current vector, L_d, L_q are direct and quadrature inductances, R is the stator winding resistance, λ_{PM} is the permanent magnet flux linkage. By discretizing equations (2) with forward-Euler approximation, the discrete-time state-space model is obtained:

$$\boldsymbol{i}_{dq}(k+1) = \boldsymbol{A}\boldsymbol{i}_{dq}(k) + \boldsymbol{B}\boldsymbol{v}_{dq}(k) + \boldsymbol{K} \tag{3}$$

with:

$$\boldsymbol{A} = \begin{bmatrix} 1-\frac{T_s R}{L_d} & \frac{p\omega_m T_s L_q}{L_d} \\ -\frac{p\omega_m T_s L_d}{L_q} & 1-\frac{T_s R}{L_q} \end{bmatrix} \boldsymbol{B} = \begin{bmatrix} \frac{T_s}{L_d} & 0 \\ 0 & \frac{T_s}{L_q} \end{bmatrix} \boldsymbol{K} = \begin{bmatrix} 0 \\ -\frac{p\omega_m T_s \lambda_{PM}}{L_q} \end{bmatrix} \tag{4}$$

where T_s is the control sampling period.

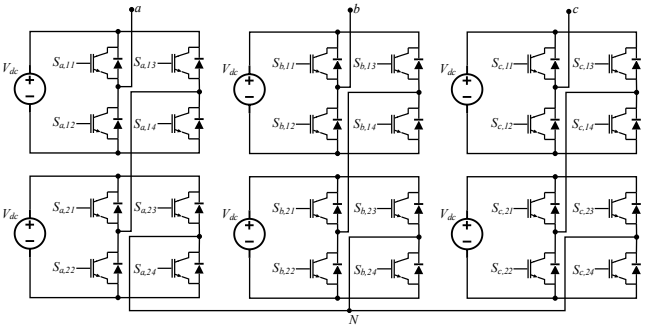

Fig. 1 Three-Phase Five-Level CHBMI circuit diagram.

By considering the 3P-5L CHBMI circuit diagram reported in Fig. 1, the CHBMI control model is obtained by expressing the inverter phase voltage v_{jN} as a function of the GCSs $S_{j,xy}$ and of the DC link voltage V_{dc} with the following relation:

$$v_{jN} = V_{dc}(S_{j,11} - S_{j,13} + S_{j,21} - S_{j,23}) \tag{5}$$

where $j \in \{A, B, C\}$ identifies the j^{th} phase, $x \in \{1, 2\}$ identifies the HB phase module, and $y \in \{1, 4\}$ identifies the HB leg. Since the inverter phase voltage $v_{xN} \in \{-2V_{dc}, -V_{dc}, 0, V_{dc}, 2V_{dc}\}$, the total number of VVs in the stationary $\alpha\beta$ reference frame $N_{v,\alpha\beta}$ is obtained as the combination of the three phases inverter voltages, according to:

$$N_{v,\alpha\beta} = n_l^m \tag{6}$$

where n_l is the number of phase voltage levels and m is the number of phases. In detail, equation (6) is equal to 125 for a 3P-5L CHBMI, and the available VVs of a 3P-5L-CHBMI in the $\alpha\beta$ reference frame are represented in Fig. 2.

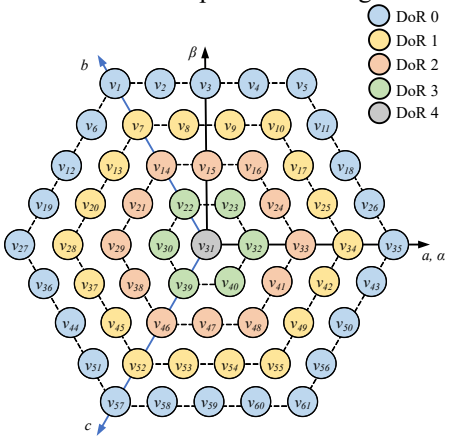

Fig. 2 CHBMI voltage vectors on the $\alpha\beta$ plane.

Fig. 2 shows that most of the available VVs are redundant, and only 61 VVs are unique. Moreover, by considering equation (5) , 125 VVs can be synthesized by 4096 GCSs combinations. Thus, the CHBMI exhibit an enormous amount of state redundancies, making the implementation of the FCS-MPC and its resolution in real time challenging. The proposed strategy considers a prediction horizon N_p=1, and the cost function J is formulated as:

$$J = \left\| \boldsymbol{i}_{dq}^{*}(k+1) - \boldsymbol{i}_{dq}(k+1) \right\|_2^2 \lambda_u \left\| \Delta \boldsymbol{v}_N(k) \right\|_1 \tag{7}$$

where $i_{dq}^{*}(k+1)=[i_d^{*}(k+1)\ i_q^{*}(k+1)]^T$ is the reference currents vector, $i_{dq}(k+1)=[i_d(k+1)\ i_q(k+1)]^T$ is the future state current vector, $\Delta v_N(k)=v_N(k)-v_N(k-1)$ is the switching effort penalization term, and λ_u is a weighting factor that can prioritize one of the two cost function terms, then directly influencing the switching frequency. In order to minimize the algorithm computational cost, an offline optimization process that eliminates VVs and GCSs redundancies is carried out. In detail, the criterion to select or discard redundant VVs and GCSs is to minimize the CMVs, the voltage phase *dv/dt*, and the GCSs transitions during a control action update. The result of this offline optimization process is a refined set of 61 non-redundant VVs, each linked to a single GCS combination. The switching constraints to be adopted online are complementary to the offline optimization process: indeed, rather than evaluating all possible control actions, the search for the optimal solution is constrained to a limited subset of VVs, specifically the previously selected optimal vector and its immediate neighbours. According to Fig. 3, this constraint lowers the number of predictions to seven.

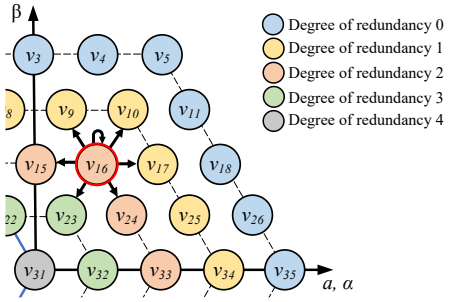

Fig. 3 Set of available voltage vectors for predictions when the previous optimal one is v_{16}, identified by the red circle.

The V²B-MPC is formulated as follows:

$$v_{ABC,opt} = \arg\min J\left(\boldsymbol{i}_{dq}(k+1), \boldsymbol{v}_{ABC}(k)\right)$$
$$subject\ to \begin{cases} \boldsymbol{i}_{dq}(k+1) = \boldsymbol{A}\boldsymbol{i}_{dq}(k) + \boldsymbol{B}\boldsymbol{T}_{dq}\boldsymbol{v}_{ABC}(k) + \boldsymbol{K} \\ \left|\Delta v_{jN}(k)\right| \le V_{DC} \\ \boldsymbol{v}_{ABC}(k) \in \boldsymbol{\mathcal{U}}(k) \end{cases} \tag{8}$$

where $\boldsymbol{\mathcal{U}}(k)$ identifies the available input variables set at the k^{th} sampling instant, which depends on the VV that is currently applied to the system. Finally, Fig. 4 shows the V²B-MPC block scheme. In detail, for practical implementation, VVs and GCSs optimized sets are stored in two dedicated Look-Up Tables (LUTs), namely LUT-1 and LUT-2, respectively.

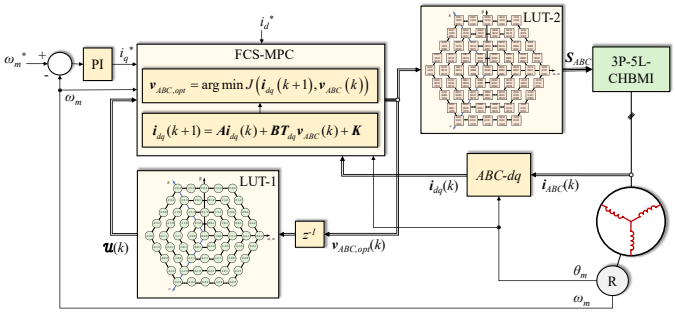

Fig. 4 V²B-MPC block scheme.

B. *Field-oriented control*

Conventional PI-based FOC with a PS-PWM [24] is chosen as the comparison target in this work. The related schematic diagram and the adopted PS-PWM modulation scheme are reported in Fig. 5 and Fig. 6, respectively.

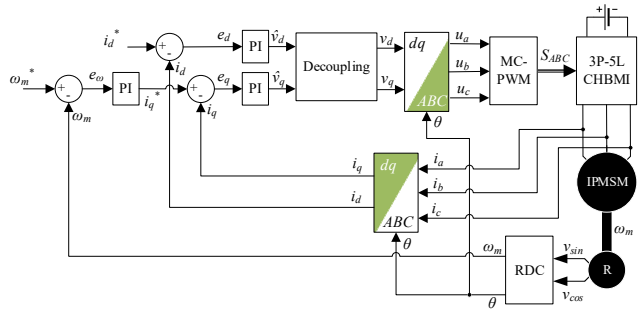

Fig. 5 Conventional PI-based FOC schematic diagram.

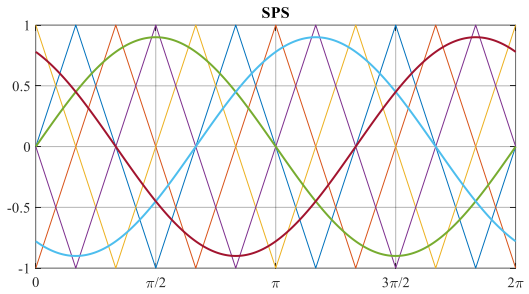

Fig. 6 Phase Shifted Pulse Width Modulation scheme.

The comparative analysis is carried out by fixing the apparent switching frequency $f_{sw,a}$ which can be evaluated as [23]:

$$f_{sw,a} = \frac{N_t}{2T_w} \tag{9}$$

where N_t is the number of phase voltage level transitions, and T_w is the observation window. Generally, for the PS-PWM strategy, the switching frequency f_{sw} coincides with the carriers frequency f_c, and they are correlated with the apparent switching frequency $f_{sw,a}$ as follows:

$$f_{sw,a} = (n_l - 1) f_{sw} \tag{10}$$

Specifically, for the 3P-5L CHBMI topology considered in this work, the apparent switching frequency is four times the device

switching frequency. It must be underlined that equation (10) stems from the characteristic of the PS-PWM modulation scheme, where the phase shift between carrier signals causes a shift in voltage harmonics across the spectrum, depending on the number of converter levels. For a given carrier frequency f_c, the modulation-induced harmonics are distributed around the apparent switching frequency and its integer multiples. A detailed description of FOC implementation is reported in [24].

III. Harmonic Power Loss Analysis Mathematical Formulation

The goal of the work is related to the detection of IPMSM efficiency and power losses defined as:

$$\eta_{PMSM}[\%] = \frac{P_m}{P_{el}} 100 \tag{11}$$

$$\Delta P_{PMSM,tot} = P_{el} - P_m \tag{12}$$

where P_m and P_{el} are the output mechanical power and the input electrical active power of the IPMSM, respectively. The electrical active power P_{el} can be calculated as a function of sampled voltage and current quantities, as:

$$P_{el} = \frac{1}{N_s} \sum_{k=0}^{N_s-1} v_k i_k \tag{13}$$

where N_s is the total number of acquired samples, v_k and i_k are the instantaneous voltage and current samples. Equivalently, P_{el} can be obtained by adopting the DFT approach [22], as follows:

$$P_{el} = P_{DC} + \sum_{h=1}^{\infty} V_h I_h \cos(\varphi_h) \tag{14}$$

where P_{DC} is the DC power component, V_h and I_h are the RMS values of h^{th} voltage and current harmonics, and φ_h is the respective phase displacement. The active power is generated by only isofrequential voltage and current harmonics, and this approach includes all harmonic components: subharmonic and interharmonic components. Thus, the total active input power $P_{el,tot}$ of a three-phase electrical motor is calculated as:

$$P_{el,tot} = P_{el,A} + P_{el,B} + P_{el,C} \tag{15}$$

The total active input power $P_{el,tot}$ can be split into the fundamental power P_1, calculated by accounting for the fundamental components of voltages and currents (h=1), and harmonic power P_h, calculated by taking into account the sum of h-order components of voltages and currents (h>1):

$$P_{el,tot} = P_1 + P_h \tag{16}$$

By assuming the high-frequency harmonics quantities have a negligible impact on the torque production, the total power losses, the relative fundamental power losses, and harmonic power losses in the motor can be determined with the following equations:

$$\Delta P_{PMSM,tot} = P_{el,tot} - P_m \tag{17}$$

$$\Delta P_{PMSM,1} = P_1 - P_m \tag{18}$$

$$\Delta P_{PMSM,h} = \Delta P_{PMSM,tot} - \Delta P_{PMSM,1} = P_{eltot} - P_{PMSM,1} \tag{19}$$

Thus, the determination of harmonic power losses requires the accurate detection of IPMSM total electric power and IPMSM fundamental electric power. The power losses quantities can be expressed in percentage value as a function of total power losses as follows:

$$\Delta P_{PMSM,1}[\%] = \frac{\Delta P_{PMSM,1}}{\Delta P_{PMSM,tot}} 100 \tag{20}$$

$$\Delta P_{PMSM,h}[\%] = \frac{\Delta P_{PMSM,h}}{\Delta P_{PMSM,tot}} 100 \tag{21}$$

For accurate detection of fundamental quantities, an observation time of 1 second and a sampling frequency of 1 MHz have been employed by obtanig a frequency resolution of 1 Hz. This choice ensures a synchronous sampling, allowing for the acquisition of an integer number of current and voltage waveform periods, which effectively reduce significantly the leakage spectrum phenomenon.

IV. Test Bench

The test bench, whose picture is reported in Fig. 1, consists of a 3P-5L CHBMI-fed IPMSM drive, whose technical data are reported in Table I and Table II. The accurate detection of IPMSM input active power is performed by a Teledyne LeCroy MDA 8038HD oscilloscope equipped with high-voltage differential probes Teledyne Lecroy HVD3106A, high-sensitivity current probe Teledyne Lecroy CP030A and a deskew calibration source DCS025 for power angle error reduction. The observation time and sampling frequency are set to 1 s and 1 MHz, respectively, by obtaining a frequency resolution of 1 Hz and synchronous sampling that results in the acquisition of an integer number of current and voltage waveform periods.

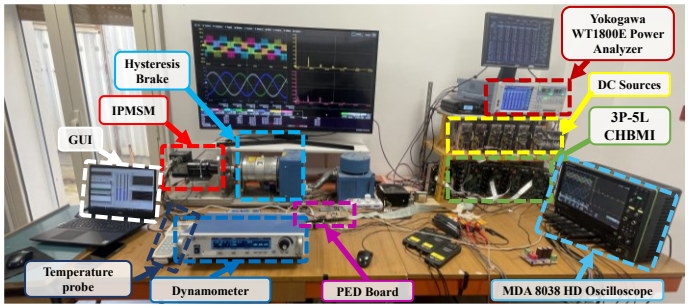

Fig. 7 Test bench.

TABLE I. IPMSM RATED DATA

Quantity	Symbol	Value
Rated Voltage	V_n	132 V
Rated current	I_n	3.6 A
Rated Speed	n	4000 rpm
Nr. of pole pairs	P	3
Nr. of phases	m	3
Rated torque	T_n	1.8 Nm

TABLE II. CHBMI MOSFET IRFB4115PBF MAIN DATA

Quantity	Symbol	Value
Voltage	V_{dss}	150 V
Resistance	R_{dSon}	9.3 mΩ
Current	I_D	104 A
Turn on delay	T_{Don}	18 ns
Rise time	T_R	73ns
Turn off delay	T_{Doff}	41 ns
Fall time	T_F	39ns
Reverse recovery	T_{RR}	86 ns
H-bridge DC-link voltage	V_{DC}	55 V
Switching frequency	f_{sw}	2-100 kHz

A Magtrol HD-715-8NA hysteresis brake is used to perform load tests, and the relative dynamometer allows the measurement of load torque and speed with the consequent determination of mechanical power. The dynamometer provides torque and speed signals that are acquired with the MDA 8038HD oscilloscope. To detect the thermal steady state condition of IPMSM during load operations, a Delta Ohm temperature probe model DO 9847 has been employed. To perform an accurate IPMSM loss maps identification, 20 WPs are defined in the motor speed-torque plane. In detail, IPMSM WPs are selected at 25%, 50%, 75%, and 100 % of the rated torque (T_n=1.8 Nm) and 5%, 25%, 50%, 75%, and 90% of the rated speed (n=4000 rpm). The defined WPs represent an extension of the WPs prescribed in the standard IEC 60034-2-3 [25], which specifies test methods and interpolation procedures for accurate inverter-fed AC motors power losses and efficiency determination. For each WP considered, the IPMSM total power losses are identified and segregated into fundamental power losses and harmonic power losses by applying the DFT approach described in the previous section. All the experimental investigations have been carried out with IPMSM at thermal equilibrium, identified following standard prescriptions [25].

V. EXPERIMENTAL RESULTS

Comparative analysis among PS-PWM-based FOC and V^{2}B-MPC is carried out by fixing the CHBMI apparent switching frequency at 1.4 kHz. As a way of example, Fig. 8 shows voltage and current trends in the time and frequency domain obtained with FOC and V^{2}B-MPC in WP3 (n=3000 rpm and T=1.8 Nm). PS-PWM-based FOC guarantees discrete voltage and current spectra, with harmonics centered around the apparent switching frequency (1.4 kHz) and its integer multiples. On the contrary, V^{2}B-MPC exhibits spectra spread across the entire frequency range. However, voltages and currents harmonics show a much lower amplitude when V^{2}B-MPC is adopted, and this coincides with a lower current ripple. By way of example, Fig. 9 shows the comparison between cumulative power trends in the frequency domain, calculated with the DFT methodology described in Section III, obtained with FOC and V^{2}B-MPC strategies in WPs1-4.

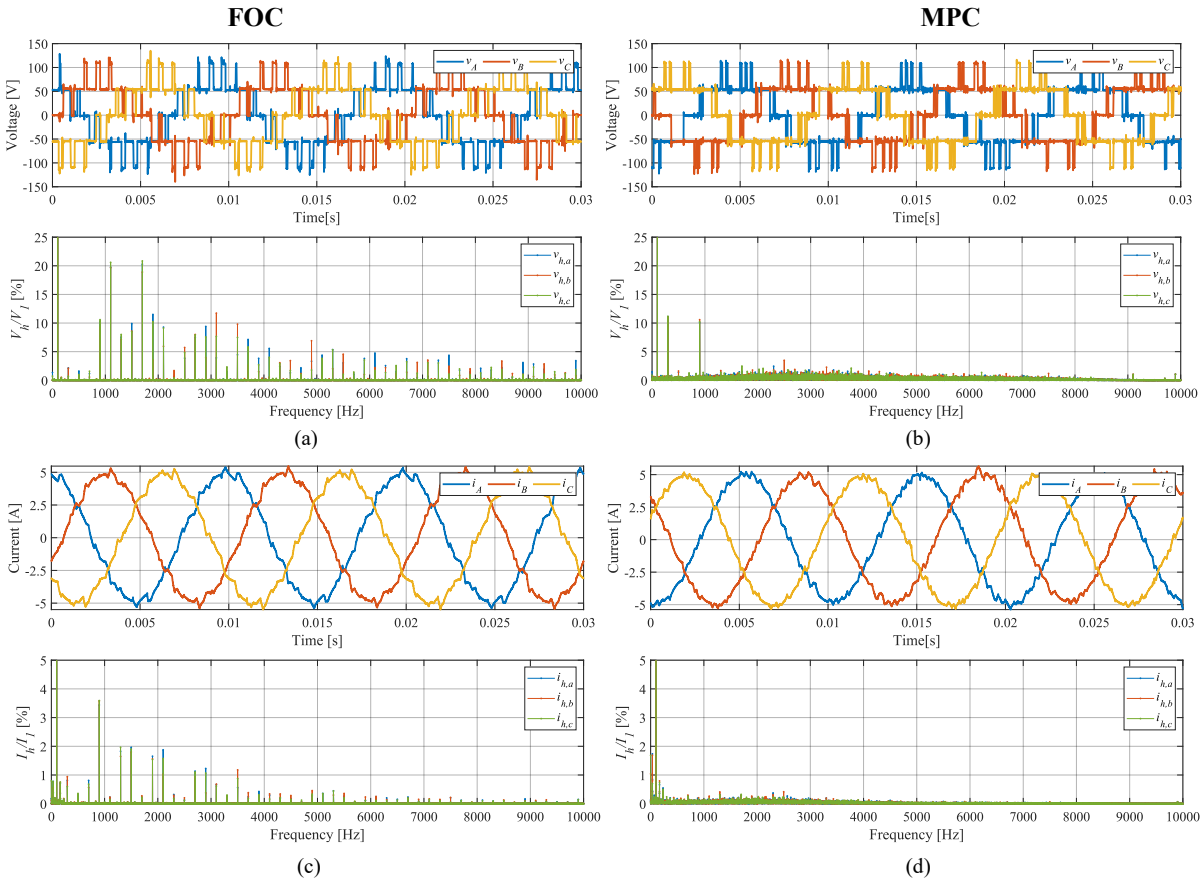

Fig. 8 Comparison between voltage and current trends in the time and frequency domain obtained with FOC (a-c) and V^{2}B-MPC (b-d) at WP3 (n=3000 rpm and T=1.8 Nm).

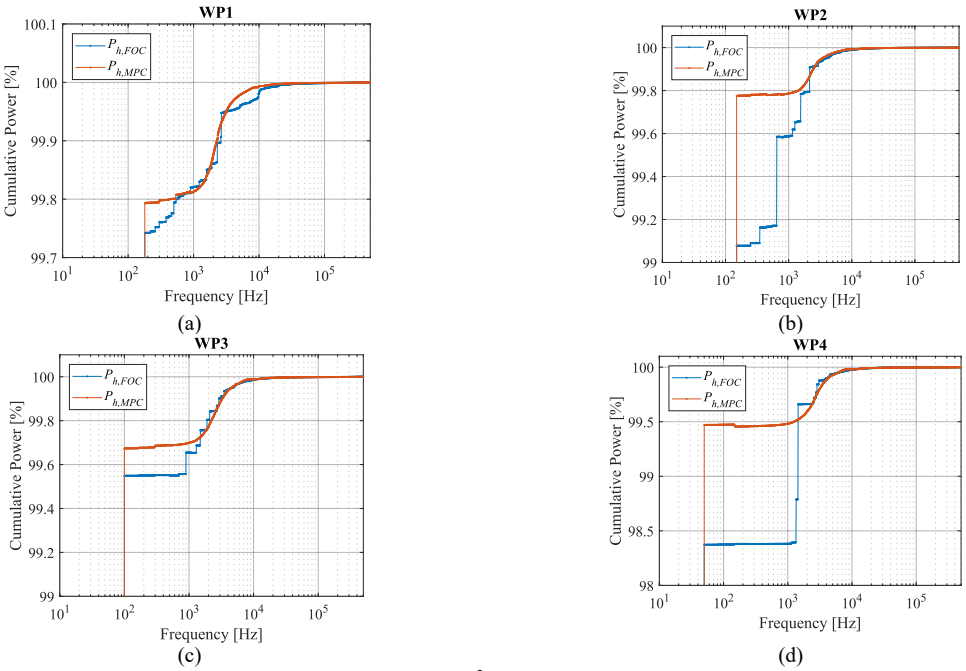

Fig. 9. Comparison between cumulative power trends obtained with FOC and V²B-MPC strategies, (a) WP1, (b) WP2, (c) WP3, (d) WP4.

TABLE III. IPMSM EFFICIENCY WITH FOC AND FCS-MPC

Efficiency η_{IPMSM} [%] - FOC					
	n [rpm]				
T [Nm]	200	1000	2000	3000	3600
1.8	24.6	58.5	71.7	76.8	78.9
1.35	30.6	63.5	75.1	78.7	80
0.9	38.8	67.4	77.1	79.2	79.7
0.45	49.6	66.5	74.2	74.3	74.1

Efficiency η_{IPMSM} [%] - MPC					
	n [rpm]				
T [Nm]	200	1000	2000	3000	3600
1.8	24.7	59.5	72	77.5	79.5
1.35	30.7	64.8	75.1	79.3	80.5
0.9	39	69.7	77.2	79.9	80.5
0.45	49.9	71	74.4	75.2	75.3

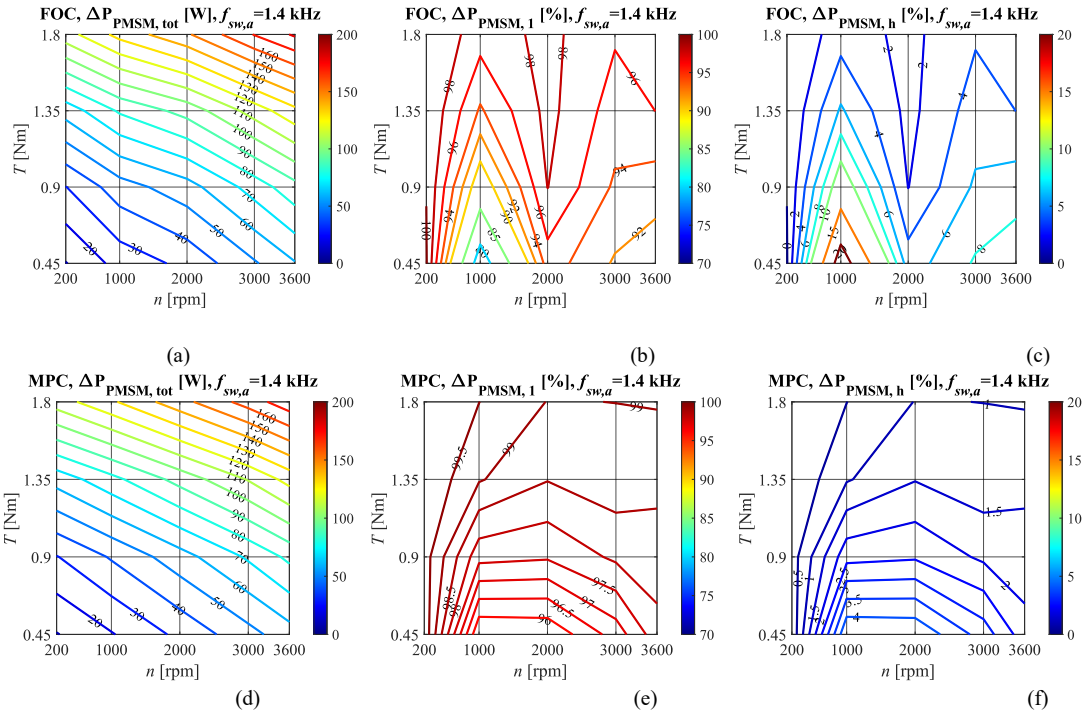

Fig. 10 Comparison between FOC and V²B-MPC: PMSM power losses (a, d), percentage fundamental power losses (b, e), and harmonic power losses (c, f).

It can be noted that V^{2}B-MPC allows for concentrating a much larger amount of power at the fundamental component, independently of the considered WP. Most relevant results are recorded at WP2 and WP4, where a difference in the fundamental power of about 1% is recorded in both cases. Moreover, the increment of cumulative power accurately reflects the harmonic behaviour of the FOC and V^{2}B-MPC strategies. In detail, the cumulative power obtained with the FOC strategy presents step variation precisely located at the frequency of voltage harmonics, i.e. apparent switching frequencies and integer multiples. Instead, the cumulative power obtained with the V^{2}B-MPC presents a continuous and smoother increase.

Tables III show a comparison between IPMSM efficiency obtained with FOC and V^{2}B-MPC over the adopted working area. It can be noted that the V^{2}B-MPC strategy guarantees the highest IPMSM efficiency in every considered WP. In detail, the efficiency difference increases as the torque load increases for a fixed mechanical speed value. The largest efficiency differences were detected at a mechanical speed equal to 1000 rpm, where V^{2}B-MPC allows to reach an increase of motor efficiency up to 4.5 % compared to the FOC strategy. Also, at a mechanical speed equal to 3600 rpm, motor efficiency increases up to 1.2 % has been detected with the use of V^{2}B-MPC compared to the conventional FOC strategy.

Fig. 10 shows the comparison between IPMSM power losses, percentage fundamental power losses, and harmonic power losses with FOC (a-c) and V^{2}B-MPC (d-f) over the adopted working area. It can be noted that the V^{2}B-MPC segregates a higher percentage of power losses at the fundamental frequency compared to the FOC. In detail, the percentage motor harmonic power losses obtained with V^{2}B-MPC are lower than 5 % in all working area considered, whereas the FOC strategy presents higher percentage motor harmonic power losses by reaching values up to 20 % at low-speed and low-torque working conditions (WPs19-20). Moreover, V^{2}B-MPC presents very low motor harmonic power losses, especially at low-speed values (200 and 1000 rpm) by reaching values lower than 1%. The behaviour of fundamental motor power losses is complementary to that described for harmonic power losses.

With regards to conventional FOC strategy, the observed behaviour of percentage motor harmonic power losses can be attributed to the fact that motor harmonic power losses are almost constant throughout the working area, and their percentage values increase at low-speed and low-torque working conditions where the motor power losses present reduced absolute values. Instead, with regards to the V^{2}B-MPC strategy, the increase of motor harmonic power losses is related only to the decrease of load torque. This highlights the correlation with the additional copper losses related to the current ripple, which presents a more significant amplitude at reduced torque load. However, as described before, the harmonic motor power losses present a very reduced amplitude when the V^{2}B-MPC is employed to control the CHBMI-IPMSM drive.

Thus, the analysis conducted demonstrates not only a better efficiency motor performance when the V^{2}B-MPC is employed but also a different behaviour in terms of power losses segregation. In detail, the IPMSM power losses are almost entirely generated by fundamental quantities throughout the working area when the V^{2}B-MPC is employed, resulting in additional margins for an overall motor efficiency improvement due to their controllability.

VI. Conclusions

In this work, an experimental comparative analysis between FOC and V^{2}B-MPC in terms of IPMSM efficiency and power losses is presented and discussed. In detail, the motor power losses are segregated into fundamental power losses and harmonic ones by the power analysis in the frequency domain with the described DFT approach. Experimental investigations have been carried out for twenty different IPMSM working points defined in the speed-torque plane at thermal steady-state conditions. Results clearly show the benefit related to the adoption of FCS-MPC for PMSM drives control purposes. In detail, the proposed V^{2}B-MPC allows to reach better motor efficiency behaviour compared to those obtained with conventional FOC strategy, and almost all motor power losses are almost entirely generated by fundamental quantities, providing additional margins for an overall motor efficiency improvement due to their controllability.

Acknowledgment

This work was supported in part by European Union—NextGenerationEU-National Sustainable Mobility Center CN00000023, Italian Ministry of University and Research Decree n. 1033—17/06/2022, Spoke 3, 12, CUP B73C22000760001, in part by the Prin 2022-Settore/Ambito di intervento: PE7 Enhanced Energy-Saving Powertrains for Freight E-Transportation (ESPFET) under Grant PRJ-0962-CUP B53D23002440006. The authors would like to acknowledge that this work was carried out in the following laboratories: Sustainable Development and Energy Saving laboratory (SDESLab), Rapid Prototyping Laboratory (RPLab), Laboratory of Electrical Applications (LEAP) at the Department of Engineering, Building no.9, University of Palermo, Italy.

References

[1] F. J. T. E. Ferreira and A. T. de Almeida, "Reducing Energy Costs in Electric-Motor-Driven Systems: Savings Through Output Power Reduction and Energy Regeneration," in *IEEE Industry Applications Magazine*, vol. 24, no. 1, pp. 84-97, Jan.-Feb. 2018.

[2] L. Aarniovuori, H. Kärkkäinen, M. Niemelä, K. Cai, J. Pyrhönen and W. Cao, "Experimental Investigation of the Losses and Efficiency of 75 kW Induction Motor Drive System," IECON 2019 - 45th Annual Conference of the IEEE Industrial Electronics Society, Lisbon, Portugal, 2019, pp. 1052-1058.

[3] Y. Shi, R. D. Lorenz, and M. A. Valenzuela, "New developments in loss minimizing control for drives without compromising torque dynamics," *IEEE Trans. Ind. Appl*., vol. 52, no. 6, pp. 5327–5335, Nov./Dec. 2016.

[4] R. Leuzzi et al., "High-Speed Machines: Typologies, Standards, and Operation Under PWM Supply," 2018 AEIT International Annual Conference, Bari, Italy, 2018, pp. 1-6.

[5] M. Caruso, A. O. Di Tommaso, M. Lombardo, R. Miceli, C. Nevoloso and C. Spataro, "Maximum Torque Per Ampere control algorithm for low saliency ratio interior permanent magnet synchronous motors," 2017 IEEE 6th International Conference on Renewable Energy Research and Applications (ICRERA), San Diego, CA, USA, 2017, pp. 1186-1191.

[6] M. Trabelsi, H. Vahedi, and H. Abu-Rub, "Review on single-DC-source multilevel inverters: Topologies, challenges, industrial applications, and

recommendations," *IEEE Open J. Ind. Electron. Soc*., vol. 2, pp. 112–127, 2021.

[7] H. Aburub, J. Holtz, and J. Rodriguez, "Medium-voltage multilevel converters-state of the art, challenges, and requirements in industrial applications," *IEEE Trans. Ind. Electron*, vol. 57, no. 8, pp. 2581–2596, Dec. 2010.

[8] H. Abu-Rub, S. Bayhan, S. Moinoddin, M. Malinowski and J. Guzinski, "Medium-Voltage Drives: Challenges and existing technology," in *IEEE Power Electronics Magazine*, vol. 3, no. 2, pp. 29-41, June 2016.

[9] F. Deng, J. Hou, Y. Zhang, M. Cheng, Y. Hu and S. Vazquez, "A Furtherance of High-Power Adjustable-Speed Drive Systems: Medium-Frequency ac Link-Powered Machine Drive Systems," in *IEEE Industrial Electronics Magazine*, vol. 17, no. 4, pp. 17-31, Dec. 2023.

[10] P. Karamanakos, E. Liegmann, T. Geyer and R. Kennel, "Model Predictive Control of Power Electronic Systems: Methods, Results, and Challenges," in *IEEE Open Journal of Industry Applications*, vol. 1, pp. 95-114, 2020.

[11] G. Scaglione, C. Nevoloso, G. Schettino, A. O. D. Tommaso and R. Miceli, "A Novel Split Space-Vector-Based Model Predictive Control With DC Power Balancing Strategy for Cascaded H-Bridge Inverter-Fed PMSM Drives," in *IEEE Transactions on Power Electronics*, vol. 39, no. 10, pp. 12826-12841, Oct. 2024.

[12] P. Karamanakos and T. Geyer, "Guidelines for the Design of Finite Control Set Model Predictive Controllers," in *IEEE Transactions on Power Electronics*, vol. 35, no. 7, pp. 7434-7450, July 2020.

[13] P. Karamanakos, E. Liegmann, T. Geyer and R. Kennel, "Model Predictive Control of Power Electronic Systems: Methods, Results, and Challenges," in *IEEE Open Journal of Industry Applications*, vol. 1, pp. 95-114, 2020.

[14] C. Nevoloso et al., "On the Inadequacy of IEC 60034-2-3 and IEC 60034-30-2 Standards for Power Losses, Efficiency and Energy Class Evaluation in PWM Multilevel Inverter-Driven PMSM," in *IEEE Open Journal of the Industrial Electronics Society*, vol. 6, pp. 962-981, 2025.

[15] L. Aarniovuori et al., "Segregation of additional high frequency harmonic losses created by PWM supply," in Proc. IEEE 65th Int. Sci. Conf. Power Elect. Eng. Riga Tech. Univ., 2024, pp. 1–6.

[16] A. Kremser, "Calculation and measurement of motor and converter losses according to IEC 61800-9-2 ED2," *Forsch Ingenieurwes*, vol. 88, 2024, Art. no. 45.

[17] T. Geyer, "A Comparison of Control and Modulation Schemes for Medium-Voltage Drives: Emerging Predictive Control Concepts Versus PWM-Based Schemes," in *IEEE Transactions on Industry Applications*, vol. 47, no. 3, pp. 1380-1389, May-June 2011

[18] J. Scoltock, T. Geyer and U. K. Madawala, "A Comparison of Model Predictive Control Schemes for MV Induction Motor Drives," in *IEEE Transactions on Industrial Informatics*, vol. 9, no. 2, pp. 909-919, May 2013.

[19] Wang, F.; Zhang, Z.; Mei, X.; Rodríguez, J.; Kennel, R. Advanced Control Strategies of Induction Machine: Field Oriented Control, Direct Torque Control and Model Predictive Control. *Energies* 2018, 11, 120.

[20] H. Hadla and F. Santos, "Performance Comparison of Field-oriented Control, Direct Torque Control, and Model-predictive Control for SynRMs," in *Chinese Journal of Electrical Engineering*, vol. 8, no. 1, pp. 24-37, March 2022.

[21] I. Harbi et al., "Model-Predictive Control of Multilevel Inverters: Challenges, Recent Advances, and Trends," in *IEEE Transactions on Power Electronics*, vol. 38, no. 9, pp. 10845-10868, Sept. 2023.

[22] L. Aarniovuori, H. Kärkkäinen, M. Niemelä and J. Pyrhönen, "PWM-Induced Harmonic Power in 75 kW IM Drive System," 2020 22nd European Conference on Power Electronics and Applications (EPE'20 ECCE Europe), Lyon, France, 2020, pp. P.1-P.9.

[23] G. Scaglione, C. Nevoloso, G. Schettino, A. O. D. Tommaso and R. Miceli, "A Novel Multiobjective Finite Control Set Model Predictive Control for IPMSM Drive Fed by a Five-Level Cascaded H-Bridge Inverter," in *IEEE Journal of Emerging and Selected Topics in Power Electronics*, vol. 12, no. 2, pp. 1959-1973, April 2024.

[24] A. O. D. Tommaso et al., "Field oriented control of IPMSM fed by multilevel cascaded H-bridges inverter with NI-SOM sbRIO-9651 FPGA controller," in Proc. Int. Symp. Power Electron., Elect. Drives, Autom. Motion, 2022, pp. 88–93.

[25] *Rotating Electrical Machines Part 2-3: Specific Test Methods for Determining the Losses and Efficiency of Converter-Fed AC Machines*, IEC Standard 60034-2-3, 2024.